

Influence of hydrostatic pressure on the structural, electronic, and optical properties of $B_xAl_yGa_{1-x-y}N$ quaternary alloys: a first-principle study

© Abdelkader Bouazza¹, M'hamed Larbi²

¹L2GEGI Laboratory, University of Tiaret,
14000 Tiaret, Algeria

²Physics Department, Djillali Liabes University,
22000 Sidi Bel-Abbes, Algeria

E-mail: abdelkader.bouazza@univ-tiaret.dz

Received June 10, 2022

Revised October 12, 2022

Accepted for publication July 17, 2023

To investigate the effects of Al-doping on the structural, electronic, and optical properties of $B_xAl_yGa_{1-x-y}N$ quaternary alloys in the zinc-blende (ZB) phase, first-principle total-energy calculations were performed using the full-potential linearized augmented plane wave (FP-LAPW) technique as implemented in the WIEN2k code, which is based on density functional theory (DFT). Different exchange correlation energy approximations were used, such as the local density approximation (LDA) and the generalized gradient approximation within the Perdew–Burke–Ernzerh (PBE-GGA) parameterization. We also used the Tran-Blaha modified Becke–Johnson (TB-mBJ) approach to determine the band structures with great precision. Under hydrostatic pressure ($P = 0$ to 30 GPa), the pressure dependency of the $B_xAl_yGa_{1-x-y}N$ with different concentrations $(x, y) = [(0.25, 0.25), (0.25, 0.50), \text{ and } (0.50, 0.25)]$ for electronic and $B_{0.50}Al_{0.25}Ga_{0.25}N$ for optical properties was also investigated. In addition, we discovered that $B_xAl_yGa_{1-x-y}N$ retains its direct band-gap energy semiconductor. Using this value range, we can get the appropriate optical characteristics for several technical applications. When these quaternary alloys are subjected to hydrostatic pressure, we notice that all energy gaps widen as the pressure rises, while the nature of the fundamental gap remains unchanged for all quaternary compounds.

Keywords: density functional theory (DFT), electronic band-structure, optical properties, semiconductors, quaternary alloys.

DOI: 10.61011/SC.2023.05.57155.3804

1. Introduction

Materials science is a broad field that includes semiconductors. This discipline has made a determined effort to develop and master new materials with substantial technological potential in recent years. III–V element semiconductors, for example, have a broad forbidden band (energy gap) and crystallize as zinc-blende. III–N nitride semiconductors and related compounds have piqued interest as important optoelectronics and electronics materials. Gallium nitride (GaN), aluminum nitride (AlN), and similar materials are of tremendous interest because of their use in visible and ultraviolet (UV) light-emitting systems. Boron nitride (BN) is an excellent contender for protective coatings due to its high melting temperature, hardness, and bulk modulus for the cubic kind. It also has good heat conductivity, making it useful for electronic devices [1–3].

Many research groups have recently become interested in the characteristics of the $B_xAl_yGa_{1-x-y}N$ quaternary solid solution. The structural, electrical, and optical properties of III–N semiconductors and their solid solutions have been studied using materials science models and computational techniques such as density functional theory (DFT). Because they have a direct band-gap, excellent chemical stability, and robust mechanical properties, blue and UV emitters, high power, electronics, and high temperature are appealing. Due to their vast band-gap, element III-nitrides are often

employed in lasers, LEDs, and UV photodetectors, and their field of application is broad, with light-emitting diodes (green, blue), display panel giants, white LEDs being widely marketed and used for illumination [4–6].

To meet the demand for new generation devices in nonlinear optics, electronics, photovoltaic detectors, light-emitting diodes, cell photodetectors, transistors, pulsed laser diodes, and as thin film materials in new technology semiconductors applications [7–15], we create new alloys by combining III–V semiconductor binary compounds, allowing us to diversify physical properties such as band-gap, mesh agreement, and dielectric constant.

It is vital to examine the physical environment in which electrons move to comprehend the many features of nitride compounds. This research focuses on calculation procedures, which can be classified into three categories:

1. Experimental data for specific parameters or quantities are used to determine the values of other quantities using empirical approaches.

2. Semi-empirical approaches rely on atomic parameters and experimental data to forecast yet-to-be-determined qualities.

3. To characterize the energy behavior of materials from the first principles ab-initio approaches are used. However, it is sufficient to know their composition to model materials from the resolution of quantum mechanics equations (they

Table 1. Adopted atomic positions of the $B_xAl_yGa_{1-x-y}N$ compound

Materials	B	Al	Ga	N
$B_{0.25}Al_{0.25}Ga_{0.50}N$	(0.00,0.00,0.00)	(0.50,0.50,0.00)	(0.50,0.00,0.50) (0.00,0.50,0.50)	(0.25,0.25,0.25) (0.75,0.75,0.25) (0.75,0.25,0.75) (0.25,0.75,0.75)
$B_{0.25}Al_{0.50}Ga_{0.25}N$	(0.00,0.00,0.00)	(0.50,0.50,0.00) (0.50,0.00,0.50)	(0.00,0.50,0.50)	(0.25,0.25,0.25) (0.75,0.75,0.25) (0.75,0.25,0.75) (0.25,0.75,0.75)
$B_{0.50}Al_{0.25}Ga_{0.25}N$	(0.00,0.00,0.00)	(0.50,0.50,0.00)	(0.50,0.00,0.50) (0.00,0.50,0.50)	(0.25,0.25,0.25) (0.75,0.75,0.25) (0.75,0.25,0.75) (0.25,0.75,0.75)

use the atomic constants as input parameters for the resolution of the Schrödinger equation).

Due to its simplification to the quantum mechanics equations, the Density Functional Theory (DFT) is an acceptable method for modeling solids among ab-initio methods. However, approximations are required because of the complexity of solids, which arises from the interaction of many particles. Therefore, in DFT's numerical application, different approximations are used [16–18].

In recent years, boron-based compounds and alloys, which offer many technological uses, have attracted much interest. Their good physical features, including low ionicities [19,20], short bond lengths, broad energy gaps, high thermal conductivities, and large resistivities [21,22], make them ideal for these applications.

Boron insertion into III–V compounds may pave the way for gap engineering in III–V alloys, particularly long-wavelength absorption materials for solar cells, coherent light emission, and detection, which can all benefit III–V optoelectronic applications.

Due to their frequent inclusion into heterostructures, aluminum-based compounds are the most critical electrical and optoelectronic materials [23,24].

The structural, electrical, and optical properties of zincblende $B_xAl_yGa_{1-x-y}N$ quaternary alloys are explored using the FP-LAPW method inside density functional theory (DFT) as implemented in the Wien2k code under hydrostatic pressure in the range of 0–30 GPa in this study. We will look at how pressure affects various factors, including lattice constants, band-gap energies, and optical properties. A thorough understanding of these features could pave the way for new technology applications.

In our case, all the structures with x composition (alloys) have been considered on the basis of the zinc-blende structure of GaN and BN compounds.

2. Calculation procedure

The structural, electrical, and optical characteristics of zinc-blende $B_xAl_yGa_{1-x-y}N$ quaternary alloys were

investigated using the FP-LAPW approach implemented within the Vienna package WIEN2k [25,26] under the context of density functional theory (DFT). For structural calculations, the exchange and correlation potentials were addressed using several approximations — the Perdew and Wang local density approximation (PW-LDA) [27] the Perdew–Burke–Ernzerhof generalized gradient approximation (PBE-GGA) [28]. In addition to the GGA and LDA approaches, we used the modified Becke–Johnson generalized gradient approximation (TB-mBJ) for the electrical characteristics [29]. The TB-mBJ method addresses the drawbacks of GGA and LDA approaches in terms of band-gap value misjudgment.

The FP-LAPW technique extends the charge density, potential, and wave function by employing spherical harmonic functions within non-overlapping spheres enclosing the plane waves basis set and atomic sites (muffin-tin spheres) in the unit cell's remaining space (interstitial regions). This approach yields band gaps close to experimental values [29,30]. The energy convergence criteria were set at 0.0001 Ry, and the $R_{MT} \times K_{MAX}$ equal to 7 was chosen for the plane wave expansion, where R_{MT} is the minimum radii of the muffin-tin spheres K_{MAX} is the wave function basis cut-off. The R_{MT} values used in all calculations are 1.35, 1.4, 1.7, and 2.1 Bohr (0.529 Å) for B, N, Al, and Ga, respectively.

The calculations were made on the basis of a zincblende structure for GaN and BN, whose atomic positions are known, while for $B_{0.25}Al_{0.25}Ga_{0.50}N$, $B_{0.25}Al_{0.50}Ga_{0.25}N$, and $B_{0.50}Al_{0.25}Ga_{0.25}N$, the positions of the different atoms are shown in the following table (Table 1).

The cut-off energy, which determines how far the core and valence states are separated, was set to 6 Ry. As a result, the valence wave functions inside muffin-tin spheres MT are enlarged up to $I_{MAX} = 10$, with $G_{MAX} = 14$ (Ry)1/2 as the plane wave cut-off value for charge density and potential. In the irreducible Brillouin zone (BZ), integrals over the Brillouin zone (BZ) are conducted up to 1000 k-points for ZB binary compounds and 350 k-points for quaternary compounds.

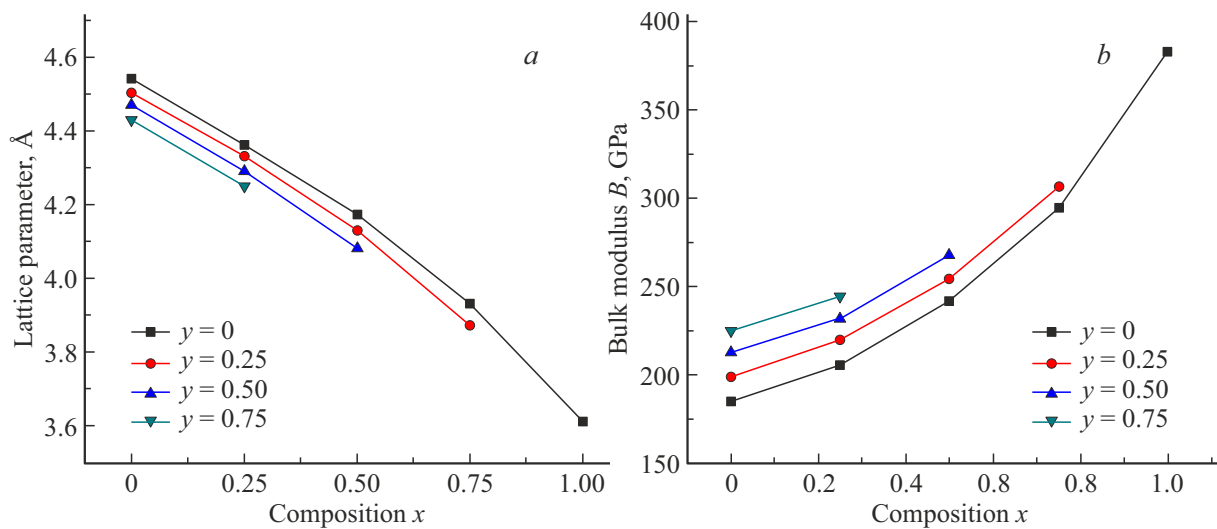


Figure 1. Lattice parameter variation (a) and Bulk modulus (b) in the Zincblende phase of $B_xAl_yGa_{1-x-y}N$ as a function of concentration y (Al) and composition x (B) calculated by GGA.

3. Results and discussion

3.1. Structural Properties

Starting with the zinc-blende (ZB) structure, we used computed forces to shift the atoms to their equilibrium positions. For simulating the structure of the quaternary solid solutions $B_xAl_yGa_{1-x-y}N$ for the considered structures and at different boron and aluminum concentrations x and y for compositions ($x = 0.25, y = 0.50$; and $x = 0.50, y = 0.25$), we chose eight atoms (in primitive P mode of fcc ZB) of $1 \times 1 \times 1$ single cells. The generalized gradient approximation GGA and LDA local density were used to calculate the structural characteristics of the Zinc-blende phase of the quaternary alloy $B_xAl_yGa_{1-x-y}N$.

For different concentrations (x) of boron and (y) of aluminum, the calculated total energies were fitted to

Table 2. Calculation of the lattice parameter a_0 (Å), the bulk modulus B (GPa), and its derivative B' (GPa) in the Zincblende phase of $B_xAl_yGa_{1-x-y}N$

Materials	Parameters	Our calculations	
		GGA	LDA
$B_{0.25}Al_{0.25}Ga_{0.50}N$	a_0 (Å)	4.33	4.27
	B (GPa)	210	230
	B' (GPa)	4.38	4.29
$B_{0.25}Al_{0.50}Ga_{0.25}N$	a_0 (Å)	4.29	4.24
	B (GPa)	213	231
	B' (GPa)	4.14	4.07
$B_{0.50}Al_{0.25}Ga_{0.25}N$	a_0 (Å)	4.13	4.08
	B (GPa)	245	264
	B' (GPa)	4.60	4.18

the Birch–Murnaghan equation of state [8] to determine ground state properties such as the equilibrium lattice parameter a_0 (Å), the bulk modulus B (GPa) and its derivative B' (GPa). Table 2 lists the structural properties of the quaternary solid solutions.

There is no experimental or theoretical evidence on the structural characteristics of the investigated solid solutions in the literature. Our findings might be used as a starting point for further study.

When experimental evidence is insufficient, it is commonly assumed, in the treatment of solid solutions, that the atoms are at their ideal positions and that the lattice characteristics vary linearly with concentration x according to Vegard's law [31,32].

Violations of this linear rule, on the other hand, have been seen both empirically [33] and conceptually for semiconductor compounds. The lattice constants of $B_xAl_yGa_{1-x-y}N$ quaternary alloy are commonly stated as a linear relation of boron composition x and aluminum composition y by the following expression, assuming Vegard's law is valid [34]:

$$a(x, y) = xa_{BN} + (y)a_{AlN} + (1 - x - y)a_{GaN}. \quad (1)$$

With varying boron and aluminum concentrations, we examined the validity of Vegard's law for the $B_xAl_yGa_{1-x-y}N$ quaternary solid solutions in the ZB structure. The composition-dependent lattice constant of these solid solutions is denoted as $a(x, y)$. The equilibrium lattice parameters of BN, AlN, and GaN are $a(BN)$, $a(AlN)$, and $a(GaN)$, respectively.

The fluctuation of the lattice parameter a_0 (Å) and the bulk modulus B (GPa) as a function of the concentration y of aluminum (Al) at different compositions x of boron (B) is shown in Fig. 1. We see a tiny discrepancy in the lattice parameter and the bulk modulus compared to Vegard's law.

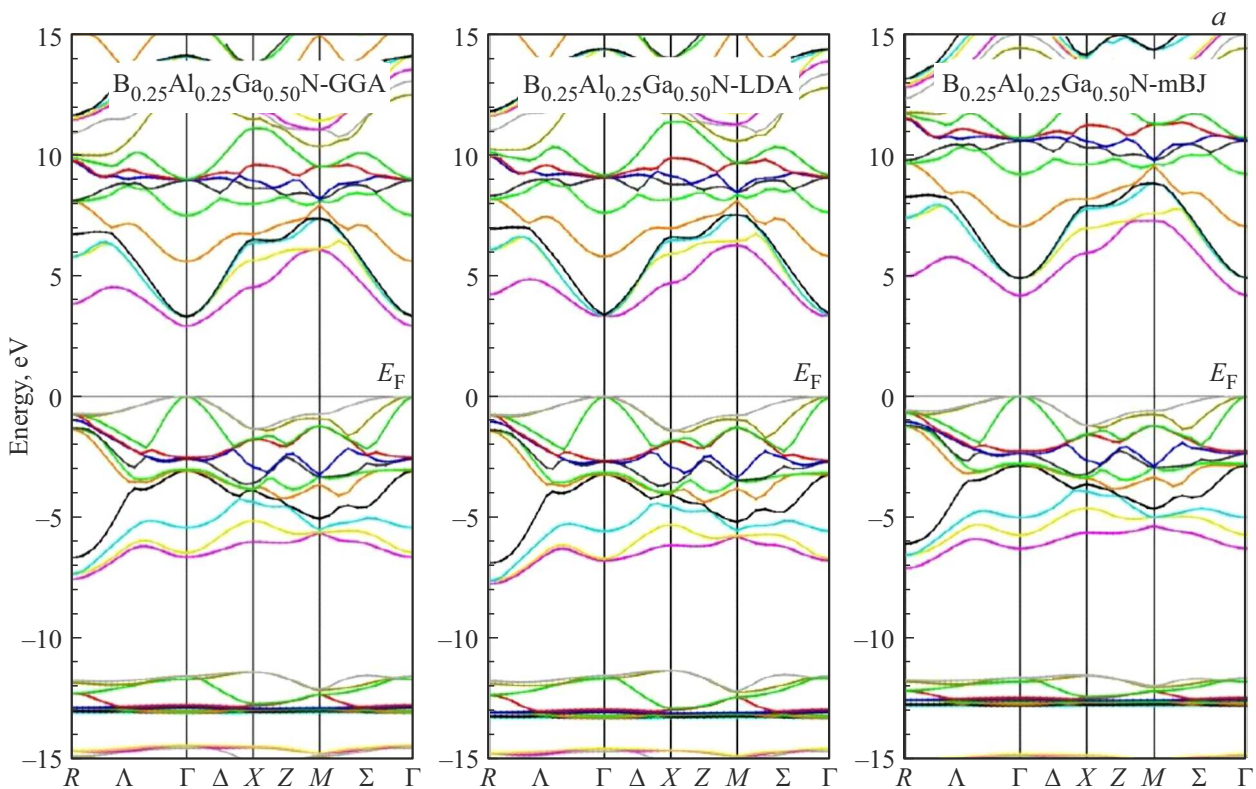


Figure 2. Band structures in the Zincblende phase calculated by GGA, LDA, and mBJ of $B_{0.25}Al_{0.25}Ga_{0.50}N$ (a), $B_{0.25}Al_{0.50}Ga_{0.25}N$ (b), and $B_{0.50}Al_{0.25}Ga_{0.25}N$ alloys.

Fig. 1, *a* shows that the lattice constant reduces approximately linearly with increasing boron concentration at a given aluminum concentration.

We can observe that at a given concentration of aluminum Al, the bulk modulus grows linearly as the concentration of B increases (see Fig. 1, *b*).

3.2. Electronic properties

3.2.1. Band structures

Based on the degree of energy band filling in their ground state, the energy band theory of solids is a way for understanding the electronic characteristics of periodic structures that enables all crystals to be classed as materials, semiconductors, insulators, or conductors [35].

The usage of quaternary alloys in optoelectronic devices has sparked much interest in studying their energy gaps. The band structure of semiconductors, whose gap width characterizes the conduction level, can be used to deduce their electrical properties.

We employed the approximations GGA, LDA, and mBJ for the potential of exchange and correlation to analyze the variance of the gaps. The GGA, LDA, and mBJ approximations were used to compute the energy bands of the $B_xAl_yGa_{1-x-y}N$ quaternary alloy. The valence band maximum and conduction band minimum are at the point of symmetry Γ for all concentrations of x and y ($x = 0.25$,

$y = 0.25$; $x = 0.25$, $y = 0.50$, and $x = 0.50$, $y = 0.25$), as shown in the Fig. 2, *a-c*.

The quaternary alloy $B_xAl_yGa_{1-x-y}N$ has a direct gap as a result. Compared to GGA and LDA, the mBJ approximation improved the gaps.

For properties dependent on the precision of the exchange and correlation potentials, the mBJ approximation yielded good results. These results are presented in Table 3.

From this Table, the maximum value of the direct gap ($\Gamma-\Gamma$) determined using the mBJ approximation for the quaternary alloy $B_xAl_yGa_{1-x-y}N$, which corresponds to ($x = 0.50$, $y = 0.25$), is equal to 4.96 eV.

Table 3. Energy calculation of the direct ($\Gamma-\Gamma$) and indirect ($\Gamma-X$) gap in the Zinc-blende phase of the quaternary compound $B_xAl_yGa_{1-x-y}N$

Compound	Energy, eV	Our calculations		
		GGA	LDA	mB
$B_{0.25}Al_{0.25}Ga_{0.50}N$	$E_{\Gamma-\Gamma}$	2.89	3.37	4.13
	$E_{\Gamma-X}$	4.50	4.68	5.90
$B_{0.25}Al_{0.50}Ga_{0.25}N$	$E_{\Gamma-\Gamma}$	3.29	3.35	4.72
	$E_{\gamma-x}$	4.84	5.01	6.28
$B_{0.50}Al_{0.25}Ga_{0.25}N$	$E_{\Gamma-x}$	3.39	3.47	4.96
	$E_{\Gamma-X}$	5.52	5.65	7.09

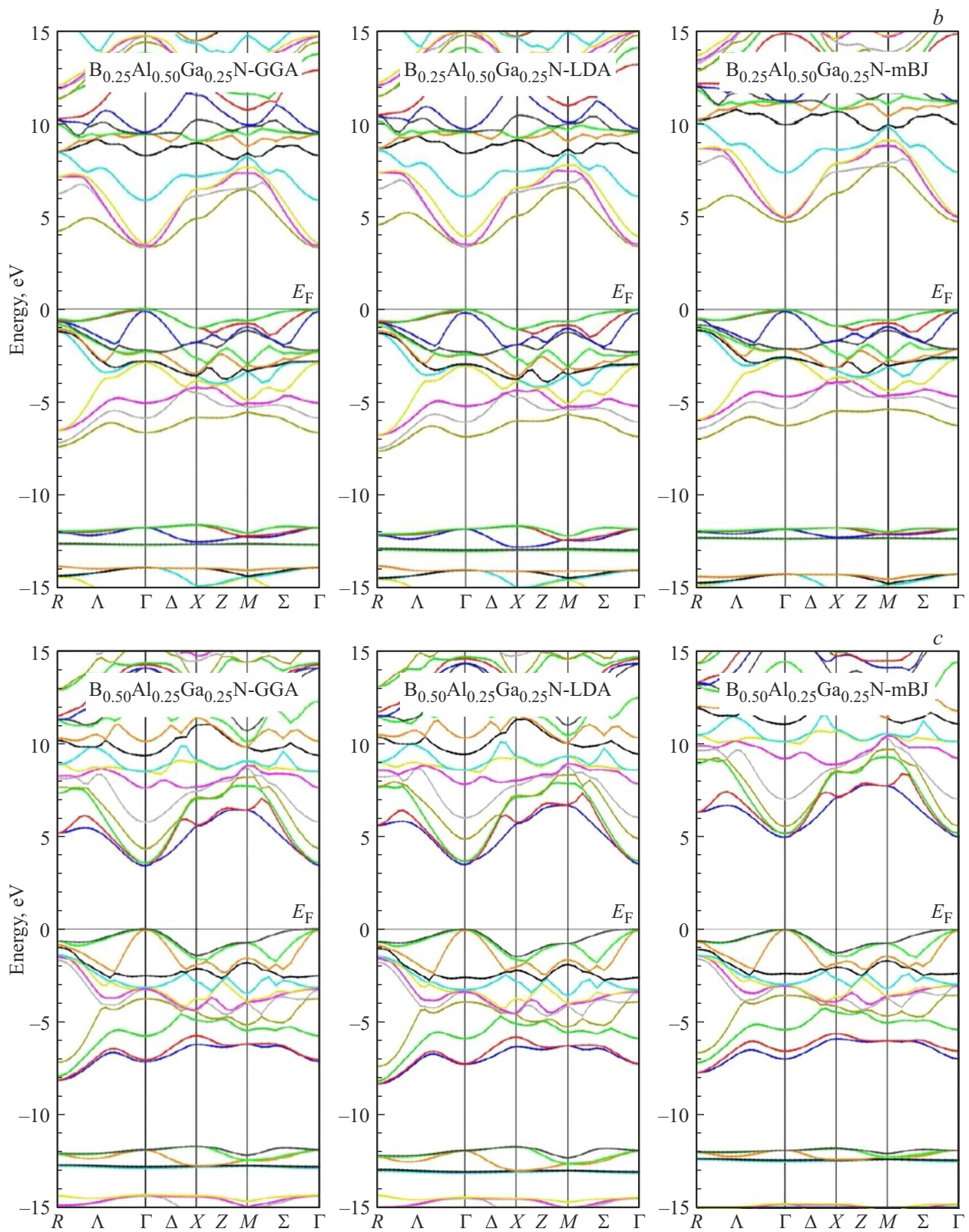


Figure 2 (continued).

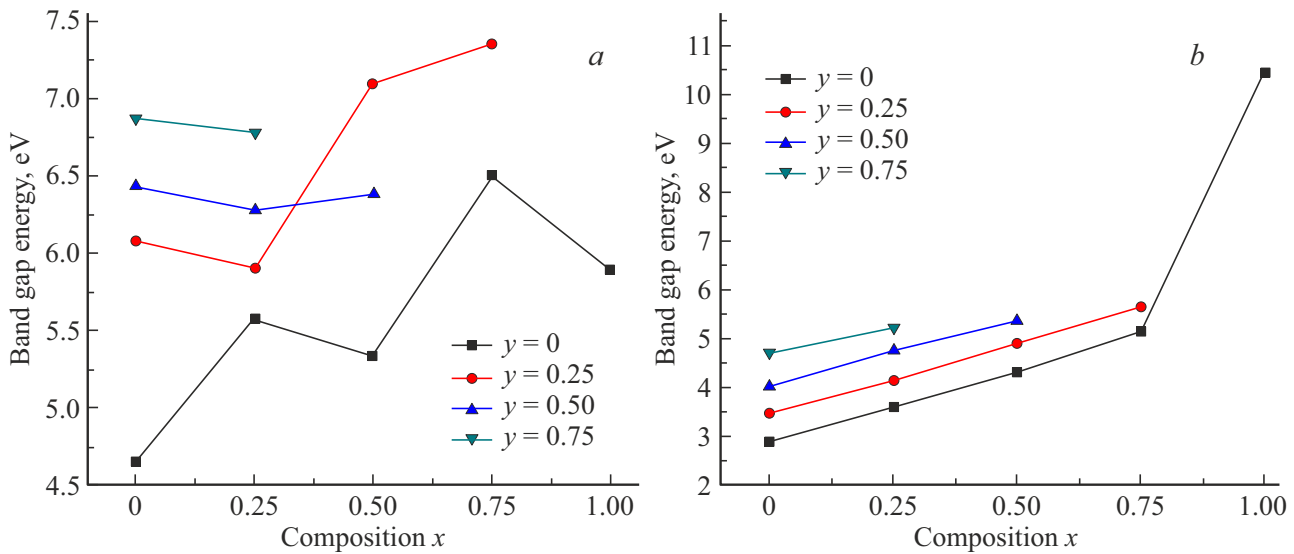


Figure 3. Variation of the direct (a), and indirect (b) band gap as a function of the concentration y and the composition x in the Zinc-blende phase of the $B_xAl_yGa_{1-x-y}N$ alloy calculated by mBJ.

Table 4. Variation of the direct and indirect gap as a function of the concentration y and the composition x of the $B_xAl_yGa_{1-x-y}N$ alloys calculated by mBJ

y	x	Compounds	$E_{\Gamma-\Gamma}$	$E_{\Gamma-x}$
0	0	GaN	2.88	4.66
	0.25	$B_{0.25}Ga_{0.50}N$	3.59	5.58
	0.50	$B_{0.50}Ga_{0.50}N$	4.7	5.34
	0.75	$B_{0.75}Ga_{0.25}N$	5.15	6.5
	1	BN	10.47	5.88
0.25	0	$Al_{0.25}Ga_{0.75}N$	3.46	6.08
	0.25	$B_{0.25}Al_{0.25}Ga_{0.50}N$	4.13	5.9
	0.50	$B_{0.50}Al_{0.25}Ga_{0.25}N$	4.9	7.09
	0.75	$B_{0.75}Al_{0.25}N$	5.65	7.35
0.50	0	$Al_{0.50}Ga_{0.50}N$	4.01	6.43
	0.25	$B_{0.25}Al_{0.50}Ga_{0.25}N$	4.72	6.28
	0.50	$B_{0.50}Al_{0.50}N$	5.36	6.38
0.75	0	$Al_{0.75}Ga_{0.25}N$	4.71	6.87
	0.25	$B_{0.25}Al_{0.75}N$	5.21	6.78

The gap energies computed with mBJ range from 4.13 to 4.96 eV. Using this range of values, we may achieve the appropriate optical characteristics for various technical applications.

The variation of the energy of the direct and indirect gap according to the concentration y ($y = 0, 0.25, 0.50$, and 0.75), and of the composition x ($x = 0, 0.25, 0.50, 0.75$, and 1) of the direct ($\Gamma-\Gamma$) and indirect ($\Gamma-X$) gap calculated using mBJ, is represented in the Fig. 3 and illustrated in Table 4.

3.2.2. State density (DOS)

The total energy of the solid, the position of the Fermi level, and the probability of electron existence all need thorough computations of the electron density of states (DOS). The entire density of states is projected onto a specific orbital of a given atom to get total and partial densities of states. Therefore, it is interesting to determine the spectra of the total and partial density of states to examine and know the type of hybridization and the states responsible for the binding to better comprehend the band structure.

The utilization of many k points in the Brillouin zone in DOS calculations necessitates a high level of precision. We used a value $k = 450$ for the Zincblende phase with various concentrations (x, y) in our calculations. The GGA approximation is used to compute the total (TDOS) and partial (PDOS) densities of states.

Fig. 4 illustrate the total and partial density of states at equilibrium in the Zincblende phase of the quaternary compounds $B_{0.25}Al_{0.25}Ga_{0.50}N$, $B_{0.25}Al_{0.50}Ga_{0.25}N$ and $B_{0.50}Al_{0.25}Ga_{0.25}N$.

Two major valence zones, VB1 and VB2, and a conduction region CB above the Fermi level can be distinguished from the origin of the energies. In the calculations, we have distinguished the core electrons B ($1s^2$), Al ($1s^2 2s^2 2p^6$), Ga ($1s^2 2s^2 2p^6 3s^2 3p^6$) and N ($1s^2$) from those of valence B ($2s^2 2p^1$), Al ($3s^2 3p^1$), Ga ($3d^{10} 4s^2 4p^1$), and N ($2s^2 2p^3$).

The first region (VB1) is located in the energy range $[-13, -11$ eV]. The [Al- $3s$, Al- $3p$, Ga- $4s$, Ga- $4p$, and N- $2s$, N- $2p$] state dominates the band VB1 for the compounds $B_{0.25}Al_{0.25}Ga_{0.50}N$, $B_{0.25}Al_{0.50}Ga_{0.25}N$, and $B_{0.50}Al_{0.25}Ga_{0.25}N$, whereas the Ga- $3d$ state contributes in VB1, [B- $2s$, Al- $3s$, Ga- $4s$, and N- $2p$] dominate the other

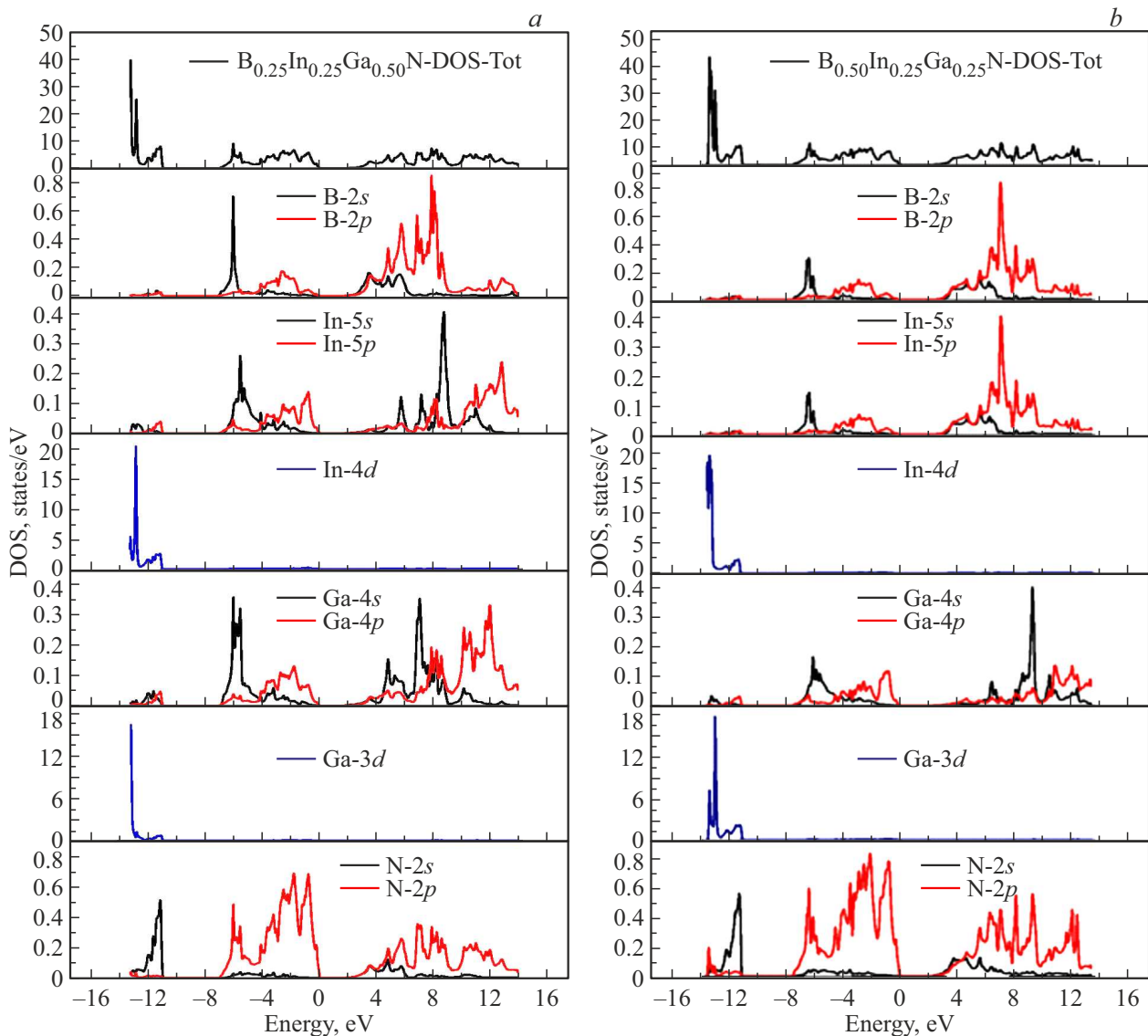


Figure 4. Total and partial density of state in the Znblende phase of $B_{0.25}Al_{0.25}Ga_{0.50}N$ (a), $B_{0.25}Al_{0.50}Ga_{0.25}N$ (b), and $B_{0.50}Al_{0.25}Ga_{0.25}N$ (c).

valence band VB2 between $[-8, 0.0\text{ eV}]$, and these are the states to the left of the contribution.

The $[B-2p, Al-3p, Ga-4p, \text{ and } N-2p]$ states are mixed in the second sub-region to the right; and the third region (CB) is predominantly dominated by $[B-2p, Al-3p, \text{ and } Ga-4p]$ for $B_{0.25}Al_{0.25}Ga_{0.50}N$; $[B-2p, Al-3p, \text{ and } Ga-4s]$ for $B_{0.25}Al_{0.50}Ga_{0.25}N$ and $[B-2p, Al-3s, \text{ and } Ga-4s]$ for $B_{0.50}Al_{0.25}Ga_{0.25}N$ with a slight contribution from the $N-2p$ states.

4. Optical properties

Optical properties in solid-state physics describe how electromagnetic radiation interacts with a substance, causing polarization effects and conduction electron movement. The dielectric function $\epsilon(\omega)$, which plays an essential role

in studying optical characteristics, can characterize these processes, which make up the material's optical response.

In this part, we have investigated and determined the optical properties of the quaternary compounds $B_xAl_yGa_{1-x-y}N$ to understand their nature better and provide a good overview of their applicability in optoelectronic devices.

The dielectric function can be used to calculate the optical properties as:

$$\epsilon(\omega) = \epsilon_1(\omega) + i\epsilon_2(\omega). \quad (2)$$

The real part $\epsilon_1(\omega)$ is associated with polarization, whereas the imaginary section $\epsilon_2(\omega)$ is determined by the electronic transition near the absorption's origin. The Kramers-Kronig relations [36–38] can be used to get the

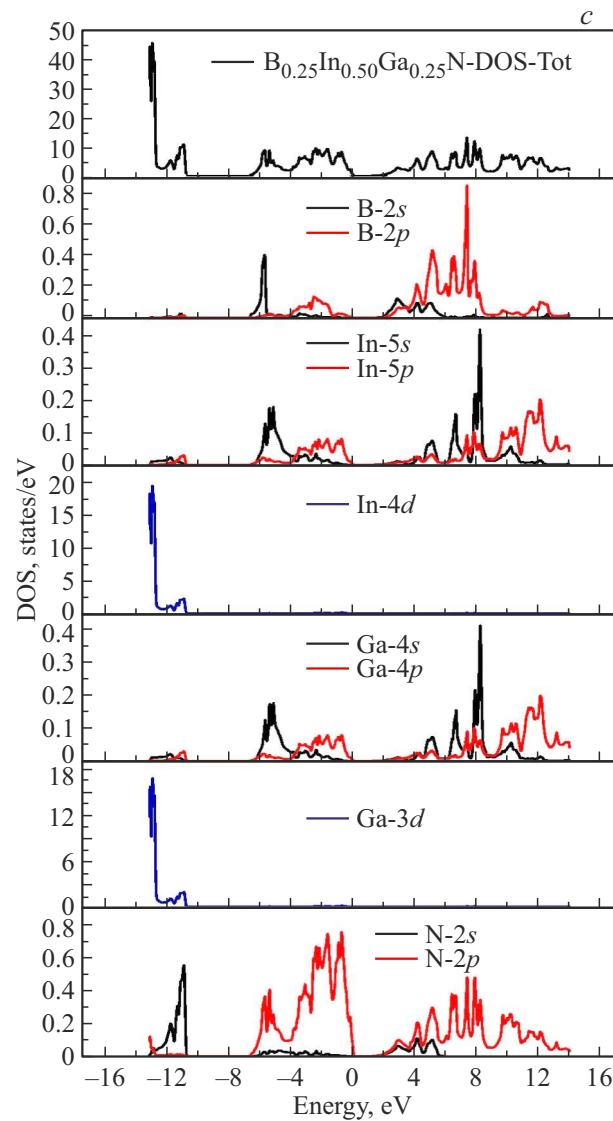


Figure 4 (continued).

real and imaginary parts of the dielectric function:

$$\varepsilon_1(\omega) = 1 + \frac{2}{\pi} P \int_0^{\infty} \frac{\omega' \varepsilon_2(\omega')}{\omega'^2 - \omega^2} d\omega', \quad (3)$$

$$\varepsilon_2(\omega) = -\frac{2\omega}{\pi} P \int_0^{\infty} \frac{\varepsilon_1(\omega') - 1}{\omega'^2 - \omega^2} d\omega'. \quad (4)$$

Where ω is the light frequency, and the primary value of the Cauchy integral is P .

The complex refractive index is one of the optical parameters that describe the interaction of light with the medium. In the construction and study of heterostructure lasers and other semiconductor waveguiding devices, knowing the refractive index of semiconductors is crucial [39].

This amount $N(\omega) = n(\omega) + ik(\omega)$ can be calculated using the real and imaginary components of the dielectric

function, with the latter defined in terms of the refractive index n and the extinction coefficient k as follows:

$$\varepsilon_1(\omega) = n^2 - k^2, \quad (5)$$

$$\varepsilon_2(\omega) = 2nk. \quad (6)$$

Where the real refractive index $n(\omega)$ and the extinction coefficient, which is also called the attenuation index $k(\omega)$ can be given by the following two relations [40,41]:

$$n(\omega) = \left[\frac{\varepsilon_1(\omega)}{2} + \frac{\sqrt{\varepsilon_1^2(\omega) + \varepsilon_2^2(\omega)}}{2} \right]^{1/2}, \quad (7)$$

$$k(\omega) = \left[\frac{\sqrt{\varepsilon_1^2(\omega) + \varepsilon_2^2(\omega)}}{2} - \frac{\varepsilon_1(\omega)}{2} \right]^{1/2}. \quad (8)$$

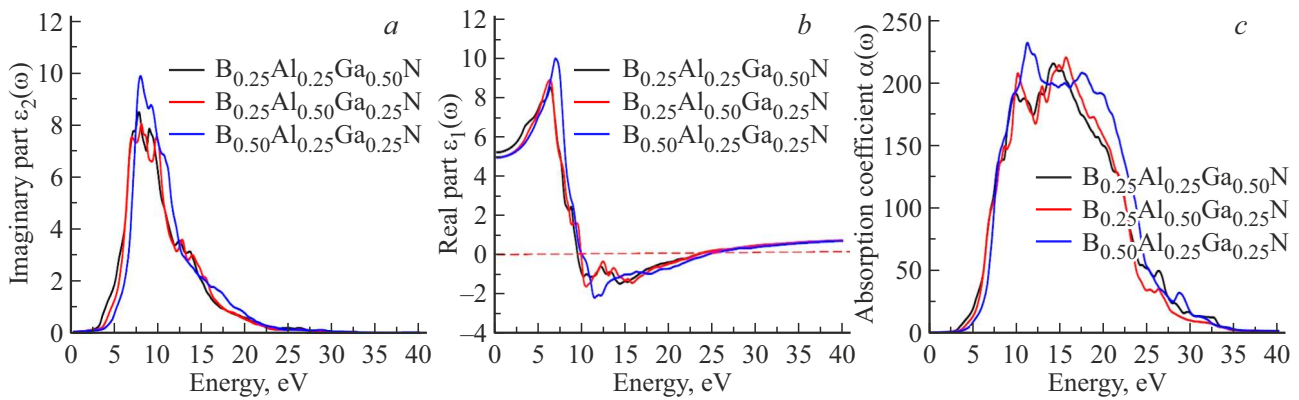


Figure 5. Variation of the dielectric function's imaginary part (a), real part (b) and the absorption coefficient $\alpha(\omega)$ (10^4 cm^{-1}) (c) as a function of energy as a function of energy for $B_{0.25}Al_{0.25}Ga_{0.50}N$, $B_{0.25}Al_{0.50}Ga_{0.25}N$ and $B_{0.50}Al_{0.25}Ga_{0.25}N$.

At low frequency ($\omega = 0$) and from relation (7), we obtain the following relation:

$$n(0) = \varepsilon^{1/2}(0). \quad (9)$$

We also calculated the refractive index using other empirical models:

1. Moss's model based on the atomic model [42]:

$$E_g n^4 = K. \quad (10)$$

2. The Herve and Vandamme model [43]:

$$n = \sqrt{1 + \left(\frac{A}{E_g + B} \right)^2} \quad (11)$$

with $A = 13.6 \text{ eV}$ and $B = 3.4 \text{ eV}$.

3. Ravindra's model [44]:

$$n = \alpha + \beta E_g. \quad (12)$$

With $\alpha = 4.084$ et $\beta = -0.62 \text{ eV}^{-1}$.

The knowledge of the two real and imaginary sections of the dielectric function makes it possible to calculate the absorption coefficient $\alpha(\omega)$ and the reflectivity $R(\omega)$ using the following relations [45]:

$$\alpha(\omega) = \frac{2\omega k(\omega)}{c} = \frac{4\pi k}{\lambda}$$

connected to ε_2 as follows

$$\alpha(\omega) = \frac{\varepsilon_2 \omega}{cn}, \quad (13)$$

$$R(\omega) = \frac{(n-1)^2 + k^2}{(n+1)^2 + k^2}. \quad (14)$$

4.1. The dielectric function and the absorption coefficient

We used the equilibrium lattice parameter and 450 k points in the Brillouin zone to calculate the optical characteristics of the quaternary compound $B_xAl_yGa_{1-x-y}N$ using

the approximation (GGA). Also, we present the fluctuations of $\varepsilon_2(\omega)$ and $\varepsilon_1(\omega)$ for the alloy investigated for the concentrations $(x, y) = [(0.25, 0.50), \text{ and } x = (0.50, 0.25)]$ on the Eqs (11,12).

The absorption is reflected in the imaginary component of the dielectric function, and the peaks that appear in graphs showing its fluctuation in relation to the energy are linked to optical transitions.

The absorption thresholds correspond to the optical gaps. The calculation results of the imaginary part $\varepsilon_2(\omega)$ of the dielectric function in the energy range from 0 to 40 eV for the quaternary compounds $B_xAl_yGa_{1-x-y}N$ are shown in the Fig. 5, a.

Analysis of these spectra shows that the behavior of $\varepsilon_2(\omega)$ for quaternary compounds is identical, with the first critical points of the dielectric function, which corresponds to the fundamental absorption thresholds starting at around 2.79, 3.30 and 3.42 eV for $B_{0.25}Al_{0.25}Ga_{0.50}N$, $B_{0.25}Al_{0.50}Ga_{0.25}N$ and $B_{0.50}Al_{0.25}Ga_{0.25}N$ respectively.

The optical transition between the highest valence band and the lowest conduction band is the source of these points, and the values of the critical points correspond to the transition $(\Gamma_v - \Gamma_c)$ for quaternary compounds.

The primary peaks, which indicate the absorption maximum, are at 7.70, 6.80, and 7.86 eV for $B_{0.25}Al_{0.25}Ga_{0.50}N$, $B_{0.25}Al_{0.50}Ga_{0.25}N$ and $B_{0.50}Al_{0.25}Ga_{0.25}N$, respectively, close to the absolute peak.

Fig. 5, b show the calculated results of the real (dispersive) ε_1 part of the dielectric function of the compound $B_xAl_yGa_{1-x-y}N$.

We can see that the absorption maximum $\alpha(\omega)$ coincides precisely with the transition to zero of $\varepsilon_1(\omega)$, i.e., where $\varepsilon_1 = 0$ and indicates the absence of dispersion. We note that the passage to zero of $\varepsilon_1(\omega)$, i.e., where $\varepsilon_1 = 0$ and which reflects the absence of dispersion, coincides perfectly with the absorption maximum $\alpha(\omega)$.

We discovered that the function $\varepsilon_1(0)$ for the $B_xAl_yGa_{1-x-y}N$ compound vanishes at the following energy values: 9.19, 9.42 and 9.73 eV for $B_{0.25}Al_{0.25}Ga_{0.50}N$, $B_{0.25}Al_{0.50}Ga_{0.25}N$ and $B_{0.50}Al_{0.25}Ga_{0.25}N$, respectively,

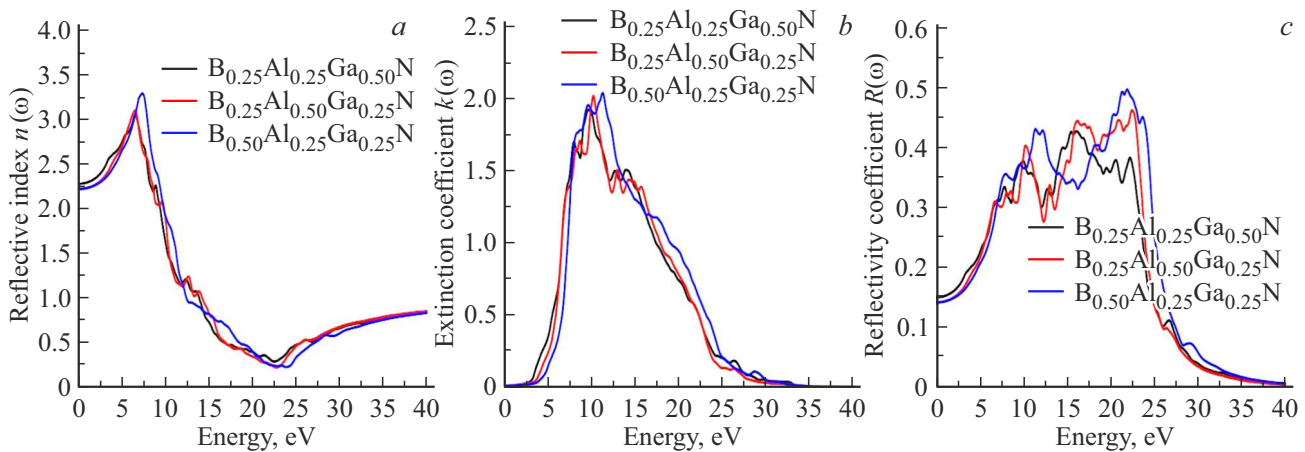


Figure 6. Variation of the refractive index $n(\omega)$ (a), the extinction coefficient $k(\omega)$ (b), and the reflectivity coefficient $R(\omega)$ (c) as a function of energy for $B_{0.25}Al_{0.25}Ga_{0.50}N$, $B_{0.25}Al_{0.50}Ga_{0.25}N$ and $B_{0.50}Al_{0.25}Ga_{0.25}N$.

Table 5. Absorption coefficient values α_0 for the quaternary compound $B_xAl_yGa_{1-x-y}N$

Compounds	Absorption coefficient α_0 (10^4 cm^{-1})
$B_{0.25}Al_{0.25}Ga_{0.50}N$	215.02
$B_{0.25}Al_{0.50}Ga_{0.25}N$	219.38
$B_{0.50}Al_{0.25}Ga_{0.25}N$	229.91

where the dispersion at these energy values is zero, and therefore the absorption is maximal.

The spectrum of the absorption coefficient $\alpha(\omega)$ for the quaternary compound $B_xAl_yGa_{1-x-y}N$ with concentrations ($x = 0.25, y = 0.25$; $x = 0.25, y = 0.50$ and $x = 0.50, y = 0.25$) is shown in Fig. 5, c. The greatest value is between 7.5 and 20 eV, and the absorption is particularly powerful in this region.

The following Table 5 groups the values of the absorption coefficient α_0 .

4.2. Refractive index, extinction coefficient and reflectivity

The Fig. 6 shows the variation of the refractive index $n(\omega)$, the extinction coefficient $k(\omega)$, and the reflectivity coefficient $R(\omega)$ as a function of energy for three quaternary compounds.

The extinction coefficient $k(\omega)$ fluctuation curves reveal multiple peaks, the most intense at 9.61, 10.12, and 11.16 eV for $B_{0.25}Al_{0.25}Ga_{0.50}N$, $B_{0.25}Al_{0.50}Ga_{0.25}N$ and $B_{0.50}Al_{0.25}Ga_{0.25}N$, respectively. These energies are the same as the energy values that cancel the spectrum of the dielectric function's real portion.

For $B_{0.25}Al_{0.25}Ga_{0.50}N$, $B_{0.25}Al_{0.50}Ga_{0.25}N$ and $B_{0.50}Al_{0.25}Ga_{0.25}N$, the maximum reflectivity is around

15.32, 22.31, and 21.79 eV, respectively. As a result, the material under investigation is an excellent option for application in the UV spectrum.

The refractive index and coefficient of reflectivity of our alloy are provided in Table 6 as static values. The results of our calculations utilizing the (GGA) approach are also included in this Table 6.

5. Pressure effect on the physical properties

5.1. Pressure effect on the electronic properties

The FP-LAPW approach within the PBE-GGA approximation was used to explore the hydrostatic pressure effect on the energy bandgap for $B_xAl_yGa_{1-x-y}N$ compounds at concentrations of ($[x = 0.25, y = 0.25]$, $[x = 0.25, y = 0.50]$, and $[x = 0.50, y = 0.25]$). To begin, the lattice constant was estimated as a function of pressure at $P = 0-30$ GPa, with a 5 GPa step, using the following equation [46]:

$$a(P) = a(0) \left[1 + \left(\frac{B'}{B} \right) P \right]^{\left(\frac{-1}{3B'} \right)} \quad (15)$$

where B is the bulk modulus, B' is the bulk modulus's pressure derivative, and $a(P)$ is the lattice parameter at the pressure P .

Using the constant lattice values deduced from Eq. (15), the direct $E(\Gamma \rightarrow \Gamma)$ and indirect $E(\Gamma \rightarrow X)$ band-gap energies of the $B_xAl_yGa_{1-x-y}N$ compounds have been calculated as a function of hydrostatic pressure. Table 7 below shows the outcomes achieved.

Fig. 7 shows the evolution of the direct and indirect band-gap energies for cubic $B_xAl_yGa_{1-x-y}N$ quaternary compounds under hydrostatic pressure.

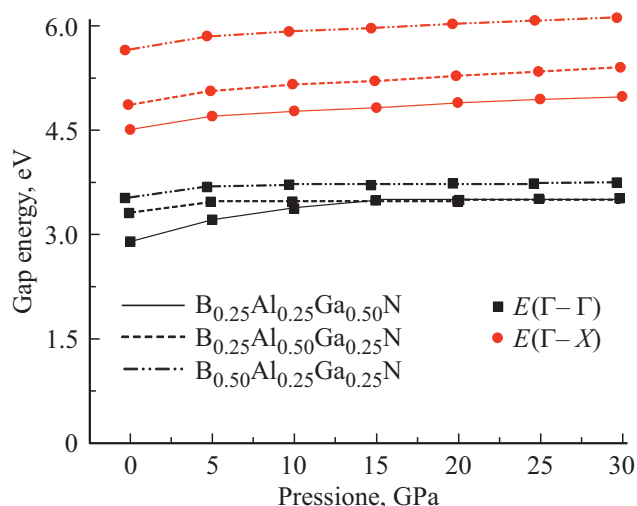
We can observe that for concentrations of ($[x = 0.25, y = 0.25]$, $[x = 0.25, y = 0.50]$, and $[x = 0.50, y = 0.25]$),

Table 6. The values of the real part $\varepsilon(0)$, the refractive index $n(0)$ and the reflectivity coefficient $R(0)$ were calculated for the two compounds $B_xAl_yGa_{1-x-y}N$

Compounds		Our calculations			
		FP-LAPW	Herve	Ravinda	Reflectivity $R(0)$
$B_{0.25}Al_{0.25}Ga_{0.50}N$	$\varepsilon(0)$	5.22	5.66	5.29	0.152
	$n(0)$	2.28	2.38	2.30	
$B_{0.25}Al_{0.50}Ga_{0.25}N$	$\varepsilon(0)$	4.94	5.15	4.16	0.143
	$n(0)$	2.22	2.27	2.04	
$B_{0.50}Al_{0.25}Ga_{0.25}N$	$\varepsilon(0)$	4.97	5.01	3.29	0.145
	$n(0)$	2.21	2.24	1.98	

Table 7. The direct and indirect band-gap energies of the $B_xAl_yGa_{1-x-y}N$ compounds at different pressures

Composition (x, y)	Band-gap energy, eV	Hydrostatic pressure P (GPa)						
		0	5	10	15	20	25	30
$B_{0.25}Al_{0.25}Ga_{0.50}N$	$E_{\Gamma-\Gamma}$	2.926	3.16575	3.345	3.46375	3.522	3.51975	3.457
	$E_{\Gamma-X}$	4.534	4.654075	4.7543	4.834675	4.8952	4.935875	4.9567
$B_{0.25}Al_{0.50}Ga_{0.25}N$	$E_{\Gamma-\Gamma}$	3.326	3.39662	3.44848	3.48158	3.49592	3.4915	3.46832
	$E_{\Gamma-X}$	4.876	5.006378	5.11751	5.209398	5.28204	5.335438	5.36959
$B_{0.50}Al_{0.25}Ga_{0.25}N$	$E_{\Gamma-\Gamma}$	3.428	3.502985	3.55794	3.592865	3.60776	3.602625	3.57746
	$E_{\Gamma-X}$	5.553	5.67324	5.77396	5.85516	5.91684	5.959	5.98164


Figure 7. The variation of the energy gaps as a function of the pressure of the compound $B_{0.25}Al_{0.25}Ga_{0.50}N$, $B_{0.25}Al_{0.50}Ga_{0.25}N$, and $B_{0.50}Al_{0.25}Ga_{0.25}N$ respectively were studied by GGA.

the direct band-gap $E(\Gamma \rightarrow \Gamma)$ and indirect band-gap $E(\Gamma \rightarrow X)$ of $B_xAl_yGa_{1-x-y}N$ quaternary compounds increases with increasing pressure in different values and that the maximum of the valence band and the minimum of the conduction band are always located on the point $\Gamma \rightarrow \Gamma$ (direct gap).

The empirical formula below is used to fit the calculated data to a quadratic function [46]:

$$E_g(P) = E_g(0) + \alpha P + \beta P^2. \quad (16)$$

Table 8 summarizes the pressure coefficients α and β obtained from the fit.

A quadratic fit from Eq. (16) is used to calculate the direct and indirect band-gap energies vs pressure of the $B_xAl_yGa_{1-x-y}N$ quaternary compounds, yielding the following results:

For $B_{0.25}Al_{0.25}Ga_{0.50}N$:

$$E_{(r-r)} = 2.926 + 0.054P - 1.21 \cdot 10^{-3}P^2 \quad (\text{Direct gap}), \quad (17)$$

$$E_{(r-x)} = 4.534 + 0.026P - 3.97 \cdot 10^{-4}P^2 \quad (\text{Indirect gap}). \quad (18)$$

For $B_{0.25}Al_{0.50}Ga_{0.25}N$:

$$E_{(r-r)} = 3.326 + 0.016P - 3.752 \cdot 10^{-4}P^2 \quad (\text{Direct gap}), \quad (19)$$

$$E_{(r-x)} = 4.876 + 0.028P - 3.849 \cdot 10^{-4}P^2 \quad (\text{Indirect gap}). \quad (20)$$

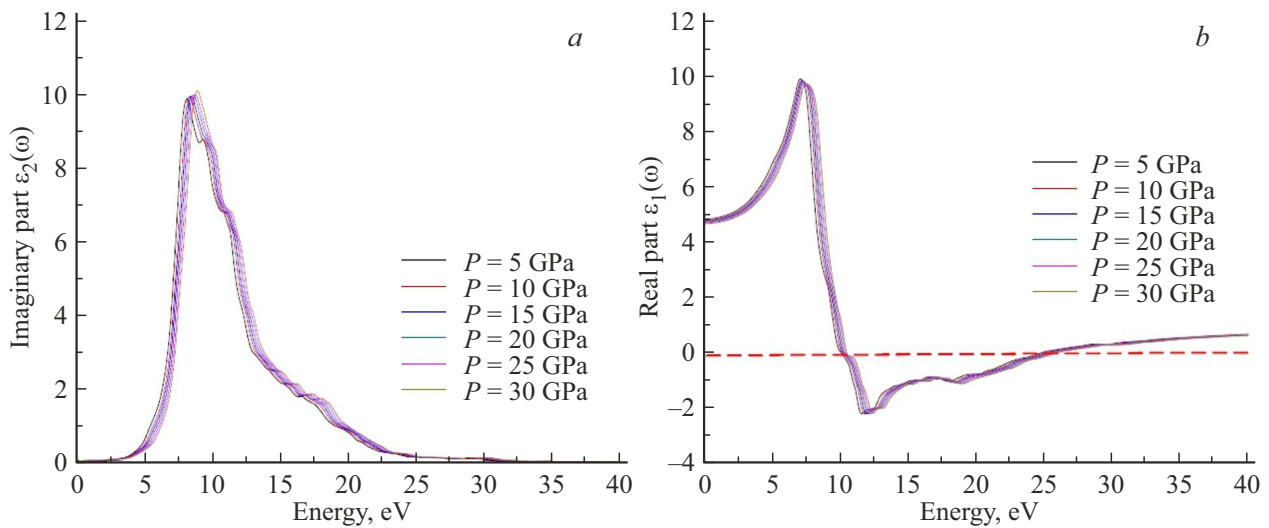
For $B_{0.50}Al_{0.25}Ga_{0.25}N$:

$$E_{(r-r)} = 3.428 + 0.017P - 4.006 \cdot 10^{-4}P^2 \quad (\text{Direct gap}), \quad (21)$$

$$E_{(r-x)} = 5.553 + 0.026P - 3.904 \cdot 10^{-4}P^2 \quad (\text{Indirect gap}). \quad (22)$$

Table 8. Hydrostatic pressure coefficients α and β for the $B_xAl_yGa_{1-x-y}N$ quaternary compounds

Composition (x, y)	Energy, eV	Our calculations	
		α (10^{-2} eV/GPa)	β (10^{-4} eV/GPa)
$B_{0.25}Al_{0.25}Ga_{0.50}N$	$E_{(r-r)}$	5.4	-0.121
	$E_{(r-x)}$	2.6	-3.97
$B_{0.25}Al_{0.50}Ga_{0.25}N$	$E_{(r-r)}$	1.6	-3.752
	$E_{(r-x)}$	2.8	-3.849
$B_{0.50}Al_{0.25}Ga_{0.25}N$	$E_{(r-r)}$	1.7	-4.006
	$E_{(r-x)}$	2.6	-3.904

**Figure 8.** The imaginary (*a*), and real (*b*) parts of the dielectric function at pressure ($P = 0-30$ GPa), corresponding to the $B_{0.50}Al_{0.25}Ga_{0.25}N$ compounds.

5.2. Pressure effect on the optical properties

We picked the combination $B_{0.50}Al_{0.25}Ga_{0.25}N$ for a concentration of ($x = 0.50, y = 0.25$) where the gap energy is more significant to explore the influence of pressure on the optical characteristics of the quaternary compound $B_xAl_yGa_{1-x-y}N$ in the zinc-blende phase using the GGA approximation.

For a pressure range of 0 to 30 GPa, we calculated the real and imaginary parts of the dielectric function, the absorption coefficient, the refractive index, the extinction coefficient, and the reflectivity.

5.2.1. The dielectric function

Pressure's effect on the dielectric function has also been investigated. The computed imaginary and real components of the dielectric function for the $B_{0.50}Al_{0.25}Ga_{0.25}N$ alloy under varied pressure values of 5, 10, 15, 20, 25, and 30 GPa are shown in Fig. 8.

Fig. 8, a shows the results of calculating the imaginary part $\epsilon_2(\omega)$ of the dielectric function for the quaternary compound in the range of 0 to 40 eV.

The positions of all peaks change to higher energies under pressure, according to the analysis of these spectra; the explanation for this is the increase in gap energies under pressure. We also observe that the prominent peaks, which reflect the absorption maximum, are located at 8.03, 8.30, 8.43, 8.56, 8.70 and 8.83 eV under the same pressure.

The calculation results of the dielectric constant $\epsilon_1(\omega)$ are represented by the Fig. 8, *b*.

The limit of the real portion of the dielectric function near-zero frequencies yields the static dielectric constant $\epsilon_1(0)$. The computed values of $\epsilon_1(0)$ for $B_{0.50}Al_{0.25}Ga_{0.25}N$ disappear at 4.86, 4.81, 4.73, 4.73, 4.62 with applicable pressures of 5, 10, 15, 20, 25, and 30 GPa, respectively, where dispersion is zero and absorption is highest.

5.2.2. Absorption coefficient

The absorption coefficient $\alpha(\omega)$ of the medium-optical measures how much light it absorbs. It is defined as the percentage of power absorbed per unit length of the medium. Fig. 9, *a* represents the variation of this coefficient for the quaternary compound $B_{0.50}Al_{0.25}Ga_{0.25}N$

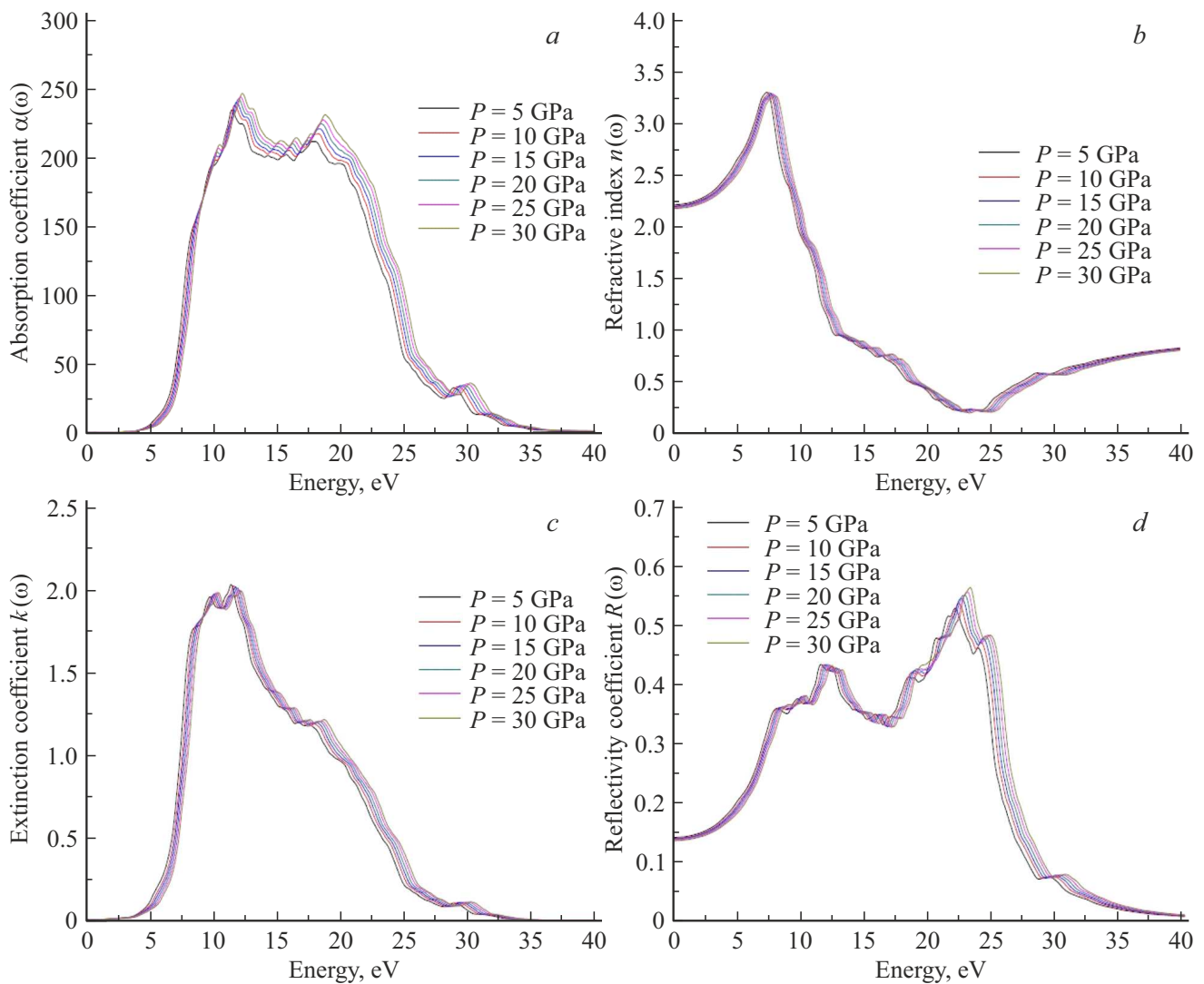


Figure 9. Variation of the absorption coefficient $\alpha(\omega)$ (10^4 cm^{-1}) (a), the refractive index $n(\omega)$ (b), the extinction index $k(\omega)$ (c), and the reflectivity coefficient $R(\omega)$ (d) as a function of energy for $B_{0.50}Al_{0.25}Ga_{0.25}N$ under pressure 5, 10, 15, 20, 25 and 30 GPa.

Table 9. The absorption coefficients α_0 values for the compound $B_{0.50}Al_{0.25}Ga_{0.25}N$ under pressure of 5, 10, 15, 20, 25 and 30 GPa

	Absorption coefficient α_0 (10^4 cm^{-1})					
	5	10	15	20	25	30
$B_{0.50}Al_{0.25}Ga_{0.25}N$	233.59	237.24	240.44	242.47	244.49	246.68

as a function of energy and pressure at 5, 10, 15, 20, 25, and 30 GPa.

There is no absorption in the low-energy zone, as can be noticed. The absorption begins around 3.87, 2.62 eV and peaks between 7.5 and 20 eV, with the absorption being assertive in this range. The absorption coefficient drops in the high energy range, where absorption is very poor for energies above 33 eV.

In Table 9 below, the values of the absorption coefficients α_0 are grouped.

5.2.3. Refractive index and extinction coefficient

The Fig. 9, b and c shows the refractive index $n(\omega)$ and extinction coefficient $k(\omega)$ for the quaternary compound $B_{0.50}Al_{0.25}Ga_{0.25}N$ generates under pressures of 5, 10, 15, 20, 25, and 30 GPa. The static values of the refractive index of our alloys are shown in Table 9.

The extinction coefficient k describes the absorption of light. The variation curves of the extinction coefficient $k(\omega)$ indicate many peaks, the most intense of which is situated at

Table 10. The values of the real part $\varepsilon(0)$, the refractive index $n(0)$ and the reflectivity coefficient $R(0)$ calculated for the $B_{0.50}Al_{0.25}Ga_{0.25}N$ under pressure range from 5 to 30 GPa

Composition		Our work (FP-LAPW)					
		5	10	15	20	25	30
$B_{0.50}Al_{0.25}Ga_{0.25}N$	$\varepsilon(0)$	4.86	4.81	4.73	4.71	4.68	4.62
	$n(0)$	2.21	2.20	2.185	2.181	2.17	2.16
	$R(0)$	0.142	0.140	0.138	0.137	0.136	0.134

11.29, 11.56, 11.81, 11.96, 12.09, and 12.21 eV, respectively, under pressures of 5, 10, 15, 20, 25, and 30 GPa.

5.2.4. Reflectivity coefficient

The reflectivity $R(\omega)$ is calculated using the refractive index $n(\omega)$ and the extinction coefficient $k(\omega)$. The variation in reflectivity as a function of energy is represented in Fig. 9, *d*.

Under pressures of 5, 10, 15, 20, 25, and 30 GPa, the calculated reflectivity reaches a maximum of roughly 22.09, 22.37, 22.49, 22.76, 23.01, and 23.26 eV.

Its maximum value remains constant across a wide range of energies until it sharply decreases at roughly 34 eV. Our alloys refractive index and reflectivity coefficient are provided in Table 6 as static values. The results of our calculations utilizing the (GGA) approach are also included in this Table 10.

6. Conclusion

This work aims to determine the influence of pressure on the structural, electronic, and optical properties of the zinc blende phase of the quaternary alloys $B_xAl_yGa_{1-x-y}N$. We used the method of linearized augmented plane waves implemented in the framework of density functional theory (DFT). The potential for exchange and correlation is handled by the local density approximation (LDA) and the generalized gradient approximation (GGA). This theoretical formalism (DFT) is implemented in the WIEN2k computer code.

We have presented only our results for quaternary compounds due to the lack of theoretical and experimental data relating to this quaternary. According to our calculations, the network parameter a_0 is undervalued by the (LDA) and inflated by the (GGA), which deviates significantly from Vegard's law. An inverse behavior concerning these two approximations is observed for the bulk modulus B .

The quaternary alloys $B_xAl_yGa_{1-x-y}N$, according to the different concentrations of x of boron and y of aluminum are directly gapped. The most significant value of the direct gap ($\Gamma-\Gamma$) calculated using the mBJ approximation are equal to 4.96 eV and 2.98 eV, which correspond to ($x = 0.50$, $y = 0.25$).

The gaps calculated using mBJ vary from 4.13 to 4.96 eV. This range of values allows us to obtain the desired optical properties for various technological applications. When these quaternary alloys are subjected to hydrostatic pressures, we notice that all the energy gaps increase with the rise in pressure and that the nature of the fundamental gap remains direct for all quaternary compounds.

Among the quantities that we also calculated, the total and partial densities of states (DOS), we noticed that the curves of the densities of states obtained by the approximation (GGA) have the same appearance. These allowed us to examine and know the contributions of the different orbitals. The densities of states show us the strong hybridization that exists between the 2p states of the B atom, (3s, 3p) of the Al atom, and (4s, 4p) of the atom Ga, as well as the 2p states of the N atom.

Finally, we theoretically explored the optical properties such as dielectric function, refractive index, extinction coefficient, and reflectivity coefficient using the method of linearized augmented plane waves (LAPW). We studied the effect of pressure on these optical properties for a concentration of $x = 0.5$ of boron and $y = 0.25$ of aluminum and this for a pressure that varies from 0 to 30 GPa. So, our studied materials are a priori good candidates for use in the ultraviolet field.

The theoretical study that we used to characterize the $B_xAl_yGa_{1-x-y}N$ quaternary allows us to have a global idea of the physical properties of this material.

Due to the lack of experimental data concerning these alloys, it is hoped that this work will make a modest contribution to this field. Our work remains to be confirmed by an experimental study to realize of components for optoelectronics.

Data Availability Statement

All relevant data are included in the paper All the data used in the manuscript are produced from the numerical simulations by the authors. No data from any external sources are used.

References

- [1] Mh. Larbi, A. Bentouaf, A. Bouazza, B. Mbarek, Aissa First principal investigation of structural, electronic and optical properties of quaternary $B_xIn_yGa_{1-x-y}N$ compounds. In: SPIN, 2020. World Scientific. <https://doi.org/10.1142/S2010324720500241>
- [2] Mh. Larbi, Riane, Rabah, Matar, F. Samir, A. Abdiche, M. Djerrouni, M. Ameri, N. Merabet, A. Oualdine. Zeitschrift für Naturforschung B, **71** (2), 125 (2016). <https://doi.org/10.1515/znb-2015-0149>
- [3] B. Bencherif, A. Abdiche, R. Moussa, R. Khenata, Xiaotian Wang. Pressure effect on structural, electronic optical and thermodynamic properties of cubic $Al_xIn_{1-x}P$: a first-principles study, Molecular Phys., **118**, 3 (2020). <https://doi.org/10.1080/00268976.2019.1608380>
- [4] M. Guemou, M. Khelil, A. Abdiche. Phys. Solid State, **62** (10), 1815 (2020). <https://doi.org/10.1134/S106378342010011X>
- [5] A. Oualdine, A. Abdiche, R. Khenata, XChinese Wang. J. Phys., **60**, 528 (2019). <https://doi.org/10.1016/j.cjph.2019.05.033>
- [6] S.-H. Jhi, J. Ihm. Phys. Status Solidi B, **191**, 387 (1995). <https://doi.org/10.1002/pssb.2221910213>
- [7] A. Bouazza. Deposition of Thin Films Materials used in Modern Photovoltaic Cells. Int. J. Thin Film Sci. Technol., **11** (3), 313 (2022). <https://doi.org/10.18576/ijfst/110308>
- [8] S.E.C. Refas, A. Bouazza, Y. Belhadji. Monte Carlo Meth. Appl., **27** (4), 373 (2021). <https://doi.org/10.1515/mcma-2021-2094>
- [9] A. Bouazza. Surf. Investigation: X-ray, Synchrotron and Neutron Techn., **16** (6), 1221 (2022). <https://doi.org/10.1134/S1027451022060283>
- [10] A. Bouazza. Sputtering of semiconductors, conductors, and dielectrics for the realization of electronics components thin-films. Int. J. Thin Film Sci. Technol., **11** (2), 225 (2022). <https://doi.org/10.18576/ijfst/110210>
- [11] A. Bouazza. 3D Visualization of the Effect of Plasma Temperature on Thin-Film Morphology. Bull. Lebedev Phys. Inst., **50** (1) 7-13 (2023). <https://doi.org/10.1134/S1027451022060283>
- [12] A. Bouazza. Investigation using Monte-Carlo codes simulations for the impact of temperatures and high pressures on thin films quality. Rev. Mex. Fis., **69** (2), 021501 1-12 (2023). <https://doi.org/10.31349/RevMexFis.69.021501>
- [13] A. Bouazza. „Revealing the role of vacuum chamber parameters on the pathways leading to substrate deposition by ejected atoms“, International Journal of Thin Film Science and Technology, vol. 12, no. 3, pp. 159-162 (2023). <https://doi.org/10.18576/ijfst/120301>
- [14] A. Bouazza. „An Investigation by Monte Carlo Simulation of the Sputtering Process in Plasma“. J. Surf. Investig. vol. 17, no. 5, 1172-1179 (2023). <https://doi.org/10.1134/S1027451023050361>
- [15] M. Koulali, A. Bouazza. „Enhancing the Sputtering Process with Plasma-Assisted Electrical Discharge for Thin Film Fabrication in Advanced Applications“, International Journal of Thin Film Science and Technology, vol. 13, no. 1, pp. 13-16 (2024). <https://doi.org/10.18576/ijfst/130102>
- [16] H. Bouafia, B. Sahli, M. Bousmaha, B. Djebour, A. Dorbane, S. Mokrane, S. Hiadsi. Solid State Sci., **118**, 106677 (2021). <https://doi.org/10.1016/j.solidstatedsci.2021.106677>
- [17] M. Bendjemai, H. Bouafia, B. Sahli, A. Dorhane, S. Uğur, G. Uğur, S. Mokrane. Phys. B: Phys. Condens. Matter, **599**, 412463 (2020). <https://doi.org/10.1016/j.physb.2020.412463>
- [18] B. Sana, H. Bouafia, M. Hassan, A. Bouaza, B. Sahli, B. Djebour, S. Hiadsi, B. Abidri. Optik, **168**, 196 (2018). <https://doi.org/10.1016/j.ijleo.2018.04.064>
- [19] J.L. He, E.D. Wu, H.T. Wang, R.P. Liu, Y.J. Tian. Phys. Rev. Lett., **94**, 015504 (2005). <https://doi.org/10.1103/PhysRevLett.94.015504>
- [20] F.El Haj Hassan, H. Akbarzadeh, M. Zoeter. J. Phys. Condens. Matter, **16**, 293 (2004). <https://doi.org/10.1088/0953-8984/16/3/009>
- [21] F. Tran, D. Koller, P. Blaha. Phys. Rev. B, **83**, 195134 (2011). <https://doi.org/10.1103/physrevb.86.134406>
- [22] C. Stampft, C.G. Van de Walle. Phys. Rev. B, **59**, 5521 (1999). <https://doi.org/10.1103/PhysRevB.59.5521>
- [23] G. Demol, T. Paulmier, D. Payan. J. Appl. Phys., **125**, 025110-1 (2019). <https://doi.org/10.1063/1.5066434>
- [24] R. Riane, R. Boussahl, Z. Zaoui, A. Hammerelaine, L. Matar. Solid State Sci., **11**, 200 (2009). <https://doi.org/10.1016/j.solidstatedsci.2008.06.001>
- [25] P. Blaha, K. Schwarz, G.K.H. Madsen, D. Kvasnicka, J. Luitz. WIEN2K: *An Augmented Plane Wave and Local Orbitals Program for Calculating Crystal Properties*, ed. by K. Schwarz (Vienna University of Technology, Austria, 2001).
- [26] J.P. Perdew, Y. Wang, Phys. Rev. B, **45** (23), 13244 (1992). <https://doi.org/10.1103/PhysRevB.45.13244>
- [27] J.P. Perdew, A. Zunger. Phys. Rev. B, **23**, 5048 (1981). <https://doi.org/10.1103/PhysRevB.23.5048>
- [28] J.P. Perdew, K. Burke. Ernzerhof **M77** (18), 3865 (1996). <https://doi.org/10.1103/PhysRevLett.77.3865>
- [29] F. Tran, P. Blaha. Phys. Rev. Lett., **102** (22), 226401 (2009). <https://doi.org/10.1103/PhysRevLett.102.226401>
- [30] D. Koller, F. Tran, P. Blaha. Phys. Rev. B, **85** (15), 155109 (2012). <https://doi.org/10.1103/PhysRevB.85.155109>
- [31] F. Bassani, M. Yoshimine. Phys. Rev., **130** (1), 20 (1963). <https://doi.org/10.1103/PhysRev.130.20>
- [32] A.R. Denton, N.W. Ashcroft. Phys. Rev. A, **43** (6), 3161 (1991). <https://doi.org/10.1103/PhysRevA.43.3161>
- [33] K. Kim, S. Limpijumngong, W.R.L. Lambrecht, B. Segall, F.A. Ponce, T.D. Moustakas, I. Akasaki, B.A. Monemar.
- [34] V.A. Fomichev, M.A. Rumsh. J. Phys. Chem. Sol., **29** (6), 1015 (1968). [https://doi.org/10.1016/0022-3697\(68\)90237-0](https://doi.org/10.1016/0022-3697(68)90237-0)
- [35] Popescu, Voicu, Alex Zunger. Phys. Rev. Lett., **104** (23), 236403 (2010). <https://doi.org/10.1103/PhysRevLett.104.236403>
- [36] S.A. Korba, H. Meradji, S. Ghemid, B. Bouhafs. Comp. Mater. Sci., **44** (4), 1265 (2009). <https://doi.org/10.1016/j.commatsci.2008.08.012>
- [37] M. ardon, Y.Y. eter. *Fundamentals of semiconductors* (Springer-Verlag, Berlin -Heidelberg, 2005) v. 619.
- [38] V. Lucarini, J.J. Saarinen, K.E. Peiponen, E.M. Vartiainen. *Kramers-Kronig relations in optical materials research* (Springer Science & Business Media, 2005) v. 110.
- [39] A. Pourghazi, M. Dadsetani. Electronic and optical properties of BaTe, BaSe and BaS from first principles. Phys. B: Condens. Matter, **370** (1–4), 35 (2005). <https://doi.org/10.1016/j.physb.2005.08.032>
- [40] S.M. Hosseini. Phys. B: Condens. Matter, **403** (10–11), 1907 (2008). <https://doi.org/10.1016/j.physb.2007.10.370>

- [41] D. Lee, A.M. Johnson, J.E. Zucker, C.A. Burrus, R.D. Feldman, R.F. Austin. *IEEE Phot. Technol. Lett.*, **4** (9), 949 (1992). <https://doi.org/10.1109/68.157111>
- [42] T.S. Moss. *Proc. Phys. Soc. Section B*, **63** (3), 167 (1950). <https://doi.org/10.1088/0370-1301/63/3/302>
- [43] P.J.L. Herve, L.K.J. Vandamme. *J. Appl. Phys.*, **77** (10), 5476 (1995). <https://doi.org/10.1063/1.359248>
- [44] N.M. Ravindra, S. Auluck, V.K. Srivastava. *Phys. Status Solidi B*, **93**(2), K155 (1979). <https://doi.org/10.1002/pssb.2220930257>
- [45] F. Wooten. *Am. J. Phys.*, **41** (7), 939 (1973). <https://doi.org/10.1119/1.1987434>
- [46] S. Adachi. *Properties of group-iv, iii-v and ii-vi semiconductors* (Wiley, West Sussex, UK, 2005).